ACS APPLIED MATERIALS & INTERFACES

Letter

www.acsami.org

Graphene-Immobilized Monomeric Bipyridine-M^{x+} (M^{x+} = Fe^{3+}, Co^{2+}, Ni^{2+}, or Cu^{2+}) Complexes for Electrocatalytic Water Oxidation

Xin Zhou,[†,‡] Teng Zhang,[†] Carter W. Abney,[†] Zhong Li,*[,‡] and Wenbin Lin*[,†]

[†]Department of Chemistry, University of Chicago, 929 E. 57th Street, Chicago, Illinois 60637, United States

[‡]School of Chemistry and Chemical Engineering, South China University of Technology, Guangzhou 510640, P.R. China

Supporting Information

ABSTRACT: Covalent anchoring of 2,2′-bipyridine (**L**) to a graphene (Gr) modified electrode followed by treatment with an $M^{x+}(NO_3)_x$ solution (M = Fe^{3+}, Co^{2+}, Ni^{2+}, or Cu^{2+}) results in surface-bound catalysts with high redox activity in neutral water at ambient temperature. Raman and IR spectroscopies indicate the successful **L** grafting and Gr deposition onto the electrodes, whereas metal concentration was determined by inductively coupled plasma mass spectrometry (ICP-MS). Cyclic voltammetry measurements were used to investigate catalytic performances, whereas a rotating ring-disk electrode was used to measure the faraday efficiencies of oxygen evolution reaction and determine experimental turnover frequencies (TOFs). Of the four metal-**L** complexes investigated, Co-**L** on a Gr-modified indium tin oxide (ITO) electrode exhibits the best catalytic activity. Washing with a solution containing catalytically inert Zn^{2+} removes Co weakly bound by surface carboxylate functionalities, and ensures the presence of only covalently attached active catalytic species. This process results in an experimental TOF of 14 s^{-1} at an overpotential of 834 mV. Functionalization of Gr-modified electrodes with appropriate metal-binding moieties thus provides a feasible strategy for loading first row transition metals onto conductive surfaces for the generation of highly active water oxidation catalysts.

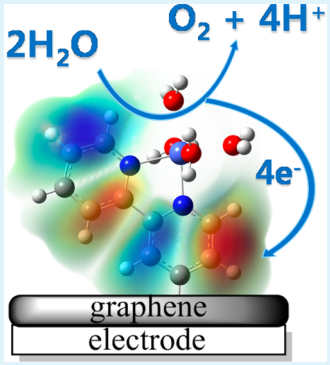

KEYWORDS: *water oxidation catalyst, 1st row transition metal, electrochemistry, graphene*

Global energy consumption is accelerating rapidly, resulting in the combustion of nonrenewable fossil fuels and emission of CO_2, one of the main sources of anthropogenic climate change. Electrolytic water splitting has become an active research area in an effort to convert electrical energy from sustainable sources to carbon-neutral fuels.[1,2] However, it is a challenging process because of the necessary stepwise transfer of multiple electrons and protons, typically resulting in a very high overpotential. Major research efforts are devoted to the development of artificial water oxidation catalysts (WOCs) as the mechanism of biological water oxidation becomes increasingly elucidated.[3−5]

The ubiquitous oxygen evolution center (OEC) of photosystem II (PS II) is widely studied as an efficient catalytic system for water oxidation. Although the active site of the OEC in PS II is a $Mn_4CaO_5(H_2O)_4$ metallocluster,[6] the most successful artificial WOCs are based on precious metals such as Ru[7−11] and Ir[12−15] whose limited supplies make them unsuitable for large-scale application. In contrast, first row transition metals are earth-abundant and inexpensive, making them feasible alternatives for WOCs. Although Fe,[16−19] Co,[20−26] Cu,[27−29] and Ni[30−35] complexes have been intensively investigated as WOCs, these molecular complexes are often unstable in the presence of strong sacrificial oxidants such as Ce(IV), periodate, or persulfate, and the identity of the actual catalyst is not always evident. It is even more problematic when the corresponding metal oxides, such as CoO_x or NiO_x, are superior WOCs compared to the initial molecular complexes.

Recently, we observed that immobilizing catalytic centers within a metal−organic framework (MOF) support can significantly enhance the catalyst stability by eliminating bimolecular decomposition pathways, resulting in highly active catalysts for water oxidation and organic reactions.[15,36] However, the insulating nature of most MOF materials prevents their applications in electrocatalysis. Graphene, a 2-dimentional sheet of carbon atoms joined by sp^2 bonds,[37] possesses high conductivity, surface area, and tunability,[38−41] making it an ideal support for immobilizing catalysts for electrochemical water oxidation.[42]

Here we report covalent anchoring of four transition metal water oxidation catalysts of the formula M-L$(H_2O)_4^{x+}$ (M= Fe^{3+}, Co^{2+}, Ni^{2+}, or Cu^{2+}, **L** = 2,2′-bipyridine) to a graphene (Gr) modified electrode (ITO or glassy carbon) to afford surface-bound catalysts with high activity in neutral water at ambient temperature. Briefly, **L** was functionalized with an amino group and grafted to graphene oxide (GO) via a diazonium coupling reaction[43,44] before electrical reduction to **L**Gr and deposition onto the electrodes to form **L**Gr-ITO. The modified electrodes were soaked in a DMF solution of the metal nitrate to metalate at the bipyridine N,N′ site, washed with deionized water and ethanol to remove weakly bound metal ions, and dried under nitrogen prior to use (Scheme 1).

Received: September 18, 2014
Accepted: October 27, 2014
Published: October 27, 2014

These Gr-bound WOC systems are referred to as **1**−**4** for Fe^{3+}, Co^{2+}, Ni^{2+}, and Cu^{2+}, respectively.

Scheme 1. Method for Covalent Attachment of 1st Row Transition Metal WOCs to Graphene-Modified ITO Electrodes

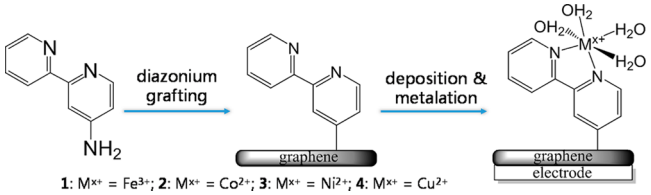

The metalated **L**Gr-modified electrode was characterized by Raman and FT-IR spectroscopy. An enhanced signal ratio I_D/I_G in the Raman spectra revealed an increase in the disorder of the Gr hexagonal network,[45] which can be attributed to covalent grafting of **L** onto Gr (Figure 1a). Similarly, FT-IR indicated the presence of **L** characteristic bands (1300−1600 cm^{-1})[46] on **L** grafted Gr (Figure 1b).

The catalytic performance of electrodes **1**−**4** was first investigated by cyclic voltammetry (CV). Figure 2 shows the voltammograms acquired in phosphate buffer (pH 7.5, 0.1 M) with KNO_3 (1 M) as supporting electrolyte. The comparison of the water oxidation current densities for the electrodes **1**−**4** shows that **2** gives the highest catalytic current density (up to 0.9 mA cm^{-2} at 1.4 V) with onset potential at ∼1.19 V vs the Ag/AgCl reference electrode, while the pristine ITO electrode gives negligible current density (22 μA cm^{-2}). In addition, **1**, **3**, and **4** also exhibit enhanced catalytic current densities compared to the pristine ITO electrode. None of the modified electrodes show visible redox couples for the metal complexes due to slow electron transfer processes at the metal centers as well as the low overall loading of surface-bound catalysts. The functionalized electrodes were digested in concentrated nitric acid and analyzed by ICP-MS to determine the exact amount of surface-bound metal sites. Turnover frequency (TOF) for the catalysts can be calculated from eq 1

$$\mathrm{TOF} = -\frac{i_a \eta}{nF\gamma} \quad (1)$$

where i_a is the catalytic current density, η is the faraday efficiency, F is Faraday's constant, γ is the surface concentration of the catalyst, and n is the number of electrons transferred per production of one oxygen molecule (n = 4). The TOFs

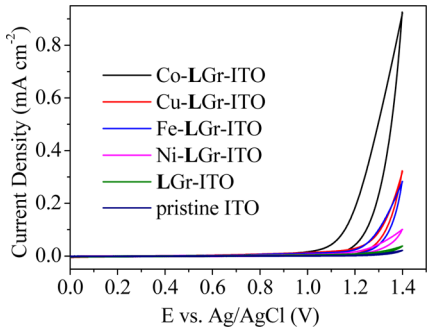

Figure 2. Comparison of CVs for **1**−**4** in phosphate buffer (pH 7.5, 0.1 M) with KNO_3 (1 M) supporting electrolyte, scan rate 50 mV s^{-1}.

reported here are calculated at 1.4 V vs Ag/AgCl (834 mV overpotential). The maximum TOF is calculated by assuming all transferred charge is used to catalyze water oxidation (η = 100%). These values are listed in Table 1. Among all four

Table 1. Maximum TOFs for the WOC Functionalized Electrodes

	M^{x+}	γ (nmol cm^{-2})	i_a (μA cm^{-2})	TOF (s^{-1})
1	Fe^{3+}	2.7 ± 0.1	245.0	0.24
2	Co^{2+}	0.9 ± 0.1	888.2	2.7
3	Ni^{2+}	1.7 ± 0.2	63.3	0.10
4	Cu^{2+}	3.6 ± 0.2	285.2	0.21

metals, Co serves as the best catalyst with a maximum TOF 1 order of magnitude higher than the other three. Thus, we focused on the Co system in the following studies.

As carboxylate functionalities are known to be present after oxidation of graphene-derived materials,[47,48] the Co^{2+} cation could also weakly bind to those sites and form $[Co\text{-}COO]^+$ species with lower catalytic activities (Figure 3). To compare

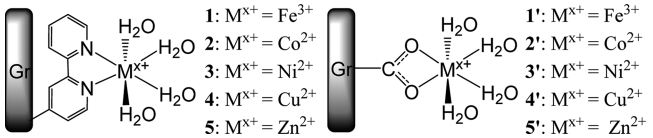

Figure 3. Proposed metal binding motifs for **L**-functionalized Gr.

the catalytic activities of $[Co\text{-}L]^{2+}$ and $[Co\text{-}COO]^+$ sites, a layer of Gr without **L** functionalization was deposited on an ITO electrode, with subsequent metalation performed as discussed

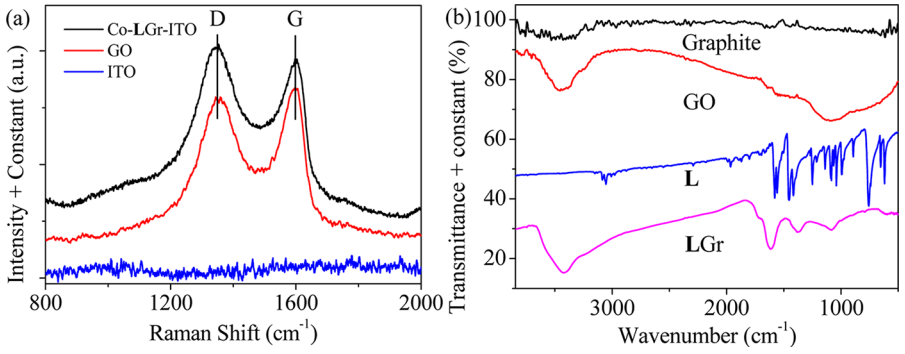

Figure 1. (a) Raman spectra of ITO, GO, and Co-LGr-ITO. I_D/I_G = 1.09 for Co-LGr-ITO, whereas I_D/I_G = 0.93 for GO. (b) FT-IR spectra of the original graphite material, graphene oxide powder (GO), ungrafted ligand **L**, and **L**-grafted GO (LGO) powder.

dx.doi.org/10.1021/am506435u | ACS Appl. Mater. Interfaces 2014, 6, 18475−18479

previously. This material, denoted **2′**, only contains Co^{2+} bound through surface carboxylate groups. Although **2′** showed higher current density than **2** (Figure 4), it also exhibited higher Co

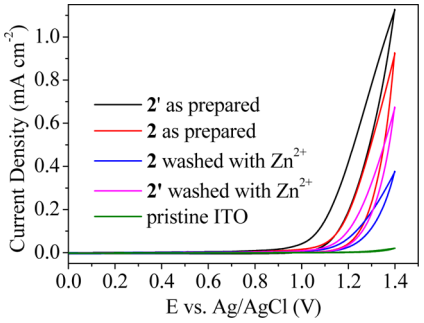

Figure 4. Comparison of CVs for Co-based catalysts **2** (Co-**L**Gr-ITO) and **2′** (Co-Gr-ITO) with and without Zn^{2+} wash. CVs were obtained in phosphate buffer (pH 7.5, 0.1 M) with KNO_3 (1 M) supporting electrolyte. Scan rate: 50 mV s^{-1}.

loading and afforded a lower TOF of 1.6 s^{-1}, revealing carboxylate-bound Co^{2+} to be an inferior WOC compared to $[Co\text{-}\mathbf{L}]^{2+}$. We expected that cation exchange with catalytically inert Zn^{2+} could displace the carboxyl-bound metals while retaining metals bound by the bipyridine functionality, resulting in better electrode performance.

Density functional theory (DFT) calculations[49] were performed to assess the feasibility of Zn^{2+} cation exchange with the weakly bound metal carboxylate species. Thermochemical calculations were performed to determine the bond strength of $[M\text{–}\mathbf{L}]^{x+}$ and $[M\text{–}COO]^{(x-1)+}$ complexes and to investigate the Gibbs free energy for Zn^{2+} substitution. As shown in Table 2, $[Zn\text{–}\mathbf{L}]^{2+}$ (**5**) is the least thermodynamically favorable of all $[M\text{–}\mathbf{L}]^{x+}$ complexes, indicating that Zn^{2+} is not likely to replace any metal ions bound by the bipyridine ligand. In contrast, $[Zn\text{-}COO]^{+}$ is more thermodynamically favorable than the Co^{2+} analogue by over 16 kJ mol^{-1}, making Zn^{2+} an ideal candidate for replacing Co^{2+} bound by COO^{-}.

Table 2. DFT Calculated Changes in Gibbs Free Energy (kJ mol^{-1}) during M^{x+} and L/COO^{-} Bond Formation

	M^{x+}	$\Delta G_{[M-L]^{x+}}$	$\Delta G_{[M-COO]^{(x-1)+}}$	$\Delta\Delta G_{[Zn-L]^{2+}}$	$\Delta\Delta G_{[Zn-COO]^{-}}$
1	Fe^{3+}	−98.81	−147.4	56.13	69.85
2	Co^{2+}	−46.43	−60.95	3.75	−16.6
3	Ni^{2+}	−84.16	−81.00	41.48	3.45
4	Cu^{2+}	−117.6	−102.3	74.92	24.75
5	Zn^{2+}	−42.68	−77.55		

As displayed in Figure 4, the anode current density of **2′** dramatically decreases after the Zn^{2+} wash, whereas **2** shows only a modest decrease. Because weakly bound $[Co\text{-}COO]^{+}$ is the catalytically active species on **2′**, it easy to reconcile the remarkable decrease in current density following Zn^{2+} wash. These results suggest the weakly bound Co^{2+} in **2′** is displaced by Zn^{2+}, which is in good agreement with the DFT results. In contrast, Zn^{2+} is not able to displace the Co^{2+} bound to **L** in **2**. Removal of the weakly bound $[Co\text{-}COO]^{+}$ results in distinct

Table 3. Maximum TOFs for Co-WOC Functionalized Electrodes

	γ (nmol cm^{-2})	I_a (μA cm^{-2})	TOF (s^{-1})
2′ as-prepared	1.8 ± 0.3	1090	1.6
2′ washed with Zn^{2+}	0.14 ± 0.04	337.2	6.1
2 as-prepared	0.86 ± 0.08	888.2	2.7
2 washed with Zn^{2+}	0.097 ± 0.004	636.5	17

improvement in catalyst activity as demonstrated by a > 14 s^{-1} increase in the maximum TOF. Before the Zn^{2+} wash, neither **2** nor **2′** exhibits a high TOF, with the anode current density of **2** attributed to the superpositioning of the catalytic currents from $[Co\text{-}\mathbf{L}]^{2+}$ and $[Co\text{-}COO]^{+}$. Following the Zn^{2+} wash, **2** exhibits outstanding catalytic activity with a maximum TOF of 17 s^{-1}, compared to 6.1 s^{-1} for Zn^{2+} washed **2′** and 2.7 s^{-1} for **2** prior to the Zn^{2+} wash. These results are consistent with our earlier hypothesis that the $[Co\text{-}\mathbf{L}]^{2+}$ site is a better WOC than the $[Co\text{-}COO]^{+}$ site.

To investigate the stability of the $[Co\text{-}\mathbf{L}]^{2+}$ catalyst system, we performed multiple CV scans with corresponding ICP-MS analyses. The current densities decreased continuously as additional CV cycles were applied (see Figure S4 in the Supporting Information), whereas ICP-MS data revealed the concentration of the surface-bound catalyst decreased as a function of number of cycles. These results indicate the catalyst system does not possess long-term stability under these conditions. Despite slow decomposition, the maximum TOF did not drop significantly (Table 4). The deteriorating

Table 4. Maximum TOFs for 2 Obtained from Sequential CV Cycles

	γ (nmol cm^{-2})	I_a (μA cm^{-2})	TOF (s^{-1})
as-prepared	0.103		
after 1 cycle	0.097	636.5	17
after 2 cycle	0.075	518.4	18
after 3 cycle	0.064	383.5	19

performance is ascribed to the gradual loss of surface-bound catalysts, rather than decomposition of the $[Co\text{-}\mathbf{L}]^{2+}$ complex. It is known that graphene-based material can be gradually oxidized at high positive potential, and oxidation and exfoliation of the graphene support may thus account for the loss of surface-bound catalysts.

To confirm the efficiency for water oxidation by **2**, we used a rotating ring-disk electrode (RRDE; Pt ring and glassy carbon disk modified with **2**) to quantify the amount of O_2 produced, affording determination of the faraday efficiency and experimental TOF. Controlled potential electrolysis was performed with the RRDE rotating at 2000 rpm in nitrogen saturated phosphate buffer (pH 7.5, 0.1M). In this measurement the disk was held at 1.4 V and the ring at −0.3 V in order to oxidize water and reduce O_2 under mass transport controlled conditions. Large bubbles of O_2 were observed after 30 min of electrolysis (see Figures S6 and S7 in the Supporting Information). Figure S8 in the Supporting Information records the current change of the electrolysis process. Current densities from the RRDE experiments are lower than those from CV scans, which can be ascribed to the gradual loss of surface-bound catalysts during bulk electrolysis, leading to a lower catalytic current density. It is worth noting this does not affect the measurement of the faraday efficiency since the ring current

is proportional to the disk current. The faraday efficiency was determined to be 82.6% calculated from eq 2

$$\eta = \frac{2\left(\int i_{\text{ring}}\mathrm{d}t - \int i'_{\text{ring}}\mathrm{d}t\right)}{\int i_{\text{disk}}\mathrm{d}t}\frac{1}{\eta_{\text{cl}}} \quad (2)$$

where i_{ring} is the current at the ring electrode, i_{disk} is the current at the modified disk electrode for electrolysis, i'_{ring} is the background current on the ring, and η_{cl} is the collecting efficiency of the RRDE ($\eta_{\text{cl}} = 0.25$). The experimental TOF for **2** was calculated as 14 s^{-1}.

In conclusion, this work demonstrates the utility of covalently anchoring first row transition metals to Gr-modified electrodes for preparation of WOC systems with high catalytic activity. Weakly bound Co^{2+} was readily removed by washing with a Zn^{2+} solution, affording a TOF of up to 14 s^{-1}. This strategy of preparing surface-immobilized WOCs facilitates investigation of electrocatalytic activities for diverse metal complexes containing simple ligands and provides a useful platform for the rapid and efficient screening of potential water oxidation catalysts.

■ ASSOCIATED CONTENT

Supporting Information

Detailed experimental process, NMR, DFT computational details, additional CVs, digit photos, and RRDE electrolysis. This material is available free of charge via the Internet at http://pubs.acs.org.

■ AUTHOR INFORMATION

Corresponding Authors

*E-mail: wenbinlin@uchicago.edu (W.L.).
*E-mail: cezhli@scut.edu.cn (Z.L.).

Author Contributions

The manuscript was written through contributions of all authors. All authors have given approval to the final version of the manuscript.

Funding

We thank National Science Foundation (DMR-1308229) for funding support. X.Z. acknowledges the financial support from the Overseas Study Program of Guangzhou Elite Project (JY201326).

Notes

The authors declare no competing financial interest.

■ ACKNOWLEDGMENTS

We thank Mr. Kuangda Lu for assistance with the Raman Spectroscopy Measurements and the University of Chicago Physical Science Division Mass Spectrometry Facility for instrumentation.

■ ABBREVIATIONS

CV, cyclic voltammetry
DFT, density functional theory
Gr, graphene
GO, graphene oxide
ICP-MS, inductively coupled plasma mass spectrometry
ITO, indium tin oxide
OEC, oxygen evolution center
PS II, photosystem II
RRDE, rotating ring disk electrode
TOF, turnover frequency
WOC, water oxidation catalyst

■ REFERENCES

(1) Karkas, M. D.; Johnston, E. V.; Verho, O.; Akermark, B. Artificial Photosynthesis: Photosynthesis: From Nanosecond Electron Transfer to Catalytic Water Oxidation. *Acc. Chem. Res.* **2014**, *47*, 100−111.
(2) Nocera, D. G. The Artificial Leaf. *Acc. Chem. Res.* **2012**, *45*, 767−776.
(3) Yagi, M.; Kaneko, M. Molecular catalysts for water oxidation. *Chem. Rev.* **2001**, *101*, 21−35.
(4) Young, K. J.; Martini, L. A.; Milot, R. L.; Snoeberger Iii, R. C.; Batista, V. S.; Schmuttenmaer, C. A.; Crabtree, R. H.; Brudvig, G. W. Light-driven water oxidation for solar fuels. *Coord. Chem. Rev.* **2012**, *256*, 2503−2520.
(5) Eisenberg, R.; Gray, H. B. Preface on making oxygen. *Inorg. Chem.* **2008**, *47*, 1697−1699.
(6) Umena, Y.; Kawakami, K.; Shen, J.-R.; Kamiya, N. Crystal structure of oxygen-evolving photosystem II at a resolution of 1.9 angstrom. *Nature* **2011**, *473*, 55−60.
(7) Duan, L.; Bozoglian, F.; Mandal, S.; Stewart, B.; Privalov, T.; Llobet, A.; Sun, L. A molecular ruthenium catalyst with water-oxidation activity comparable to that of photosystem II. *Nat. Chem.* **2012**, *4*, 418−423.
(8) Concepcion, J. J.; Jurss, J. W.; Templeton, J. L.; Meyer, T. J. One Site is Enough. Catalytic Water Oxidation by $[Ru(tpy)(bpm)(OH_2)]^{2+}$ and $[Ru(tpy)(bpz)(OH_2)]^{2+}$. *J. Am. Chem. Soc.* **2008**, *130*, 16462−16463.
(9) Sartorel, A.; Miro, P.; Salvadori, E.; Romain, S.; Carraro, M.; Scorrano, G.; Di Valentin, M.; Llobet, A.; Bo, C.; Bonchio, M. Water Oxidation at a Tetraruthenate Core Stabilized by Polyoxometalate Ligands: Experimental and Computational Evidence To Trace the Competent Intermediates. *J. Am. Chem. Soc.* **2009**, *131*, 16051−16053.
(10) Zong, R.; Thummel, R. P. A new family of Ru complexes for water oxidation. *J. Am. Chem. Soc.* **2005**, *127*, 12802−12803.
(11) Wada, T.; Tsuge, K.; Tanaka, K. Syntheses and redox properties of bis(hydroxoruthenium) complexes with quinone and bipyridine ligands. Water-oxidation catalysis. *Inorg. Chem.* **2001**, *40*, 329−337.
(12) Hull, J. F.; Balcells, D.; Blakemore, J. D.; Incarvito, C. D.; Eisenstein, O.; Brudvig, G. W.; Crabtree, R. H. Highly Active and Robust Cp* Iridium Complexes for Catalytic Water Oxidation. *J. Am. Chem. Soc.* **2009**, *131*, 8730−8731.
(13) McDaniel, N. D.; Coughlin, F. J.; Tinker, L. L.; Bernhard, S. Cyclometalated iridium(III) aquo complexes: Efficient and tunable catalysts for the homogeneous oxidation of water. *J. Am. Chem. Soc.* **2008**, *130*, 210−217.
(14) Sivasankar, N.; Weare, W. W.; Frei, H. Direct Observation of a Hydroperoxide Surface Intermediate upon Visible Light-Driven Water Oxidation at an Ir Oxide Nanocluster Catalyst by Rapid-Scan FT-IR Spectroscopy. *J. Am. Chem. Soc.* **2011**, *133*, 12976−12979.
(15) Wang, C.; Wang, J.-L.; Lin, W. Elucidating Molecular Iridium Water Oxidation Catalysts Using Metal-Organic Frameworks: A Comprehensive Structural, Catalytic, Spectroscopic, and Kinetic Study. *J. Am. Chem. Soc.* **2012**, *134*, 19895−19908.
(16) Ellis, W. C.; McDaniel, N. D.; Bernhard, S.; Collins, T. J. Fast Water Oxidation Using Iron. *J. Am. Chem. Soc.* **2010**, *132*, 10990−10991.
(17) Fillol, J. L.; Codola, Z.; Garcia-Bosch, I.; Gomez, L.; Jose Pla, J.; Costas, M. Efficient water oxidation catalysts based on readily available iron coordination complexes. *Nat. Chem.* **2011**, *3*, 807−813.
(18) Chen, G.; Chen, L.; Ng, S.-M.; Man, W.-L.; Lau, T.-C. Chemical and Visible-Light-Driven Water Oxidation by Iron Complexes at pH 7−9: Evidence for Dual-Active Intermediates in Iron-Catalyzed Water Oxidation. *Angew. Chem., Int. Ed.* **2013**, *52*, 1789−1791.
(19) Hong, D.; Mandal, S.; Yamada, Y.; Lee, Y.-M.; Nam, W.; Llobet, A.; Fukuzumi, S. Water Oxidation Catalysis with Nonheme Iron Complexes under Acidic and Basic Conditions: Homogeneous or Heterogeneous? *Inorg. Chem.* **2013**, *52*, 9522−9531.
(20) Han, X.-B.; Zhang, Z.-M.; Zhang, T.; Li, Y.-G.; Lin, W.; You, W.; Su, Z.-M.; Wang, E.-B. Polyoxometalate-Based Cobalt-Phosphate

Molecular Catalysts for Visible Light-Driven Water Oxidation. *J. Am. Chem. Soc.* **2014**, *136*, 5359−5366.
(21) Kanan, M. W.; Nocera, D. G. In situ formation of an oxygen-evolving catalyst in neutral water containing phosphate and Co^{2+}. *Science* **2008**, *321*, 1072−1075.
(22) Surendranath, Y.; Kanan, M. W.; Nocera, D. G. Mechanistic Studies of the Oxygen Evolution Reaction by a Cobalt-Phosphate Catalyst at Neutral pH. *J. Am. Chem. Soc.* **2010**, *132*, 16501−16509.
(23) Wang, D.; Groves, J. T. Efficient water oxidation catalyzed by homogeneous cationic cobalt porphyrins with critical roles for the buffer base. *Proc. Natl. Acad. Sci. U.S.A.* **2013**, *110*, 15579−15584.
(24) Yin, Q.; Tan, J. M.; Besson, C.; Geletii, Y. V.; Musaev, D. G.; Kuznetsov, A. E.; Luo, Z.; Hardcastle, K. I.; Hill, C. L. A Fast Soluble Carbon-Free Molecular Water Oxidation Catalyst Based on Abundant Metals. *Science* **2010**, *328*, 342−345.
(25) Jiao, F.; Frei, H. Nanostructured Cobalt Oxide Clusters in Mesoporous Silica as Efficient Oxygen-Evolving Catalysts. *Angew. Chem., Int. Ed.* **2009**, *48*, 1841−1844.
(26) Wasylenko, D. J.; Ganesamoorthy, C.; Borau-Garcia, J.; Berlinguette, C. P. Electrochemical evidence for catalytic water oxidation mediated by a high-valent cobalt complex. *Chem. Commun.* **2011**, *47*, 4249−4251.
(27) Zhang, T.; Wang, C.; Liu, S.; Wang, J.-L.; Lin, W. A Biomimetic Copper Water Oxidation Catalyst with Low Overpotential. *J. Am. Chem. Soc.* **2014**, *136*, 273−281.
(28) Barnett, S. M.; Goldberg, K. I.; Mayer, J. M. A soluble copper-bipyridine water-oxidation electrocatalyst. *Nat. Chem.* **2012**, *4*, 498−502.
(29) Chen, Z.; Meyer, T. J. Copper(II) Catalysis of Water Oxidation. *Angew. Chem., Int. Ed.* **2013**, *52*, 700−703.
(30) Gong, M.; Li, Y.; Wang, H.; Liang, Y.; Wu, J. Z.; Zhou, J.; Wang, J.; Regier, T.; Wei, F.; Dai, H. An Advanced Ni-Fe Layered Double Hydroxide Electrocatalyst for Water Oxidation. *J. Am. Chem. Soc.* **2013**, *135*, 8452−8455.
(31) Kenney, M. J.; Gong, M.; Li, Y.; Wu, J. Z.; Feng, J.; Lanza, M.; Dai, H. High-Performance Silicon Photoanodes Passivated with Ultrathin Nickel Films for Water Oxidation. *Science* **2013**, *342*, 836−840.
(32) Gao, M.; Sheng, W.; Zhuang, Z.; Fang, Q.; Gu, S.; Jiang, J.; Yan, Y. Efficient Water Oxidation Using Nanostructured alpha-Nickel-Hydroxide as an Electrocatalyst. *J. Am. Chem. Soc.* **2014**, *136*, 7077−7084.
(33) Liao, P.; Keith, J. A.; Carter, E. A. Water Oxidation on Pure and Doped Hematite (0001) Surfaces: Prediction of Co and Ni as Effective Dopants for Electrocatalysis. *J. Am. Chem. Soc.* **2012**, *134*, 13296−13309.
(34) Smith, R. D. L.; Prevot, M. S.; Fagan, R. D.; Zhang, Z.; Sedach, P. A.; Siu, M. K. J.; Trudel, S.; Berlinguette, C. P. Photochemical Route for Accessing Amorphous Metal Oxide Materials for Water Oxidation Catalysis. *Science* **2013**, *340*, 60−63.
(35) Hong, D.; Yamada, Y.; Nagatomi, T.; Takai, Y.; Fukuzumi, S. Catalysis of Nickel Ferrite for Photocatalytic Water Oxidation Using $Ru(bpy)_3^{2+}$ and $S_2O_8^{2}$. *J. Am. Chem. Soc.* **2012**, *134*, 19572−19575.
(36) Manna, K.; Zhang, T.; Lin, W. Postsynthetic Metalation of Bipyridyl-Containing Metal−Organic Frameworks for Highly Efficient Catalytic Organic Transformations. *J. Am. Chem. Soc.* **2014**, *136*, 6566−6569.
(37) Geim, A. K.; Novoselov, K. S. The rise of graphene. *Nat. Mater.* **2007**, *6*, 183−191.
(38) Bekyarova, E.; Itkis, M. E.; Ramesh, P.; Berger, C.; Sprinkle, M.; de Heer, W. A.; Haddon, R. C. Chemical Modification of Epitaxial Graphene: Spontaneous Grafting of Aryl Groups. *J. Am. Chem. Soc.* **2009**, *131*, 1336−1337.
(39) Paulus, G. L. C.; Wang, Q. H.; Strano, M. S. Covalent Electron Transfer Chemistry of Graphene with Diazonium Salts. *Acc. Chem. Res.* **2013**, *46*, 160−170.
(40) Zhai, Y.; Dou, Y.; Zhao, D.; Fulvio, P. F.; Mayes, R. T.; Dai, S. Carbon Materials for Chemical Capacitive Energy Storage. *Adv. Mater.* **2011**, *23*, 4828−4850.
(41) Li, X.; Wang, X.; Zhang, L.; Lee, S.; Dai, H. Chemically derived, ultrasmooth graphene nanoribbon semiconductors. *Science* **2008**, *319*, 1229−1232.
(42) Guo, S. X.; Liu, Y. P.; Lee, C. Y.; Bond, A. M.; Zhang, J.; Geletiib, Y. V.; Hill, C. L. Graphene-Supported $\{Ru_4O_4(OH)_2(H_2O)_4\}$-$(\gamma$-$SiW_{10}O_{36})_2^{10-}$ for Highly Efficient Electrocatalytic Water Oxidation. *Energy Environ. Sci.* **2013**, *6*, 2654−2663.
(43) Gomberg, M.; Bachmann, W. E. The synthesis of biaryl compounds by means of the diazo reaction. *J. Am. Chem. Soc.* **1924**, *46*, 2339−2343.
(44) deKrafft, K. E.; Wang, C.; Xie, Z.; Su, X.; Hinds, B. J.; Lin, W. Electrochemical Water Oxidation with Carbon-Grafted Iridium Complexes. *ACS Appl. Mater. Interfaces* **2012**, *4*, 608−613.
(45) Zhou, Y.; Bao, Q.; Tang, L. A. L.; Zhong, Y.; Loh, K. P. Hydrothermal Dehydration for the "Green" Reduction of Exfoliated Graphene Oxide to Graphene and Demonstration of Tunable Optical Limiting Properties. *Chem. Mater.* **2009**, *21*, 2950−2956.
(46) Gerasimova, T. P.; Katsyuba, S. A. Bipyridine and phenanthroline IR-spectral bands as indicators of metal spin state in hexacoordinated complexes of Fe(II), Ni(II), and Co(II). *Dalton Trans.* **2013**, *42*, 1787−1797.
(47) Stankovich, S.; Dikin, D. A.; Piner, R. D.; Kohlhaas, K. A.; Kleinhammes, A.; Jia, Y.; Wu, Y.; Nguyen, S. T.; Ruoff, R. S. Synthesis of graphene-based nanosheets via chemical reduction of exfoliated graphite oxide. *Carbon* **2007**, *45*, 1558−1565.
(48) Zhou, X.; Huang, W.; Shi, J.; Zhao, Z.; Xia, Q.; Li, Y.; Wang, H.; Li, Z. A novel MOF/graphene oxide composite GrO@MIL-101 with high adsorption capacity for acetone. *J. Mater. Chem. A* **2014**, *2*, 4722−4730.
(49) Frisch, M. J.; Trucks, G. W.; Schlegel, H. B.; Scuseria, G. E.; Robb, M. A.; Cheeseman, J. R.; Scalmani, G.; Barone, V.; Mennucci, B.; Petersson, G. A.; Nakatsuji, H.; Caricato, M.; Li, X.; Hratchian, H. P.; Izmaylov, A. F.; Bloino, J.; Zheng, G.; Sonnenberg, J. L.; Hada, M.; Ehara, M.; Toyota, K.; Fukuda, R.; Hasegawa, J.; Ishida, M.; Nakajima, T.; Honda, Y.; Kitao, O.; Nakai, H.; Vreven, T.; Montgomery, J. A., Jr.; Peralta, J. E.; Ogliaro, F.; Bearpark, M.; Heyd, J. J.; Brothers, E.; Kudin, K. N.; Staroverov, V. N.; Kobayashi, R.; Normand, J.; Raghavachari, K.; Rendell, A.; Burant, J. C.; Iyengar, S. S.; Tomasi, J.; Cossi, M.; Rega, N.; Millam, J. M.; Klene, M.; Knox, J. E.; Cross, J. B.; Bakken, V.; Adamo, C.; Jaramillo, J.; Gomperts, R.; Stratmann, R. E.; Yazyev, O.; Austin, A. J.; Cammi, R.; Pomelli, C.; Ochterski, J. W.; Martin, R. L.; Morokuma, K.; Zakrzewski, V. G.; Voth, G. A.; Salvador, P.; Dannenberg, J. J.; Dapprich, S.; Daniels, A. D.; Farkas, O.; Foresman, J. B.; Ortiz, J. V.; Cioslowski, J.; Fox, D. J. *Gaussian 09*; Gaussian, Inc.: Wallingford, CT, 2009.